Mechanism of the Schiff Base Forming Fructose-1,6-bisphosphate Aldolase: Structural Analysis of Reaction Intermediates‡

Esben Lorentzen,§ Bettina Siebers,|| Reinhard Hensel,|| and Ehmke Pohl*,§

European Molecular Biology Laboratory, Hamburg Outstation, Notkestrasse 85, D-22603 Hamburg, and Department of Microbiology, University of Duisburg-Essen, Universitätsstrasse 5, D-45117 Essen, Germany

Received August 20, 2004; Revised Manuscript Received December 21, 2004

ABSTRACT: The glycolytic enzyme fructose-1,6-bisphosphate aldolase (FBPA) catalyzes the reversible cleavage of fructose 1,6-bisphosphate to glyceraldehyde 3-phosphate and dihydroxyacetone phosphate. Catalysis of Schiff base forming class I FBPA relies on a number of intermediates covalently bound to the catalytic lysine. Using active site mutants of FBPA I from *Thermoproteus tenax*, we have solved the crystal structures of the enzyme covalently bound to the carbinolamine of the substrate fructose 1,6-bisphosphate and noncovalently bound to the cyclic form of the substrate. The structures, determined at a resolution of 1.9 Å and refined to crystallographic *R* factors of 0.148 and 0.149, respectively, represent the first view of any FBPA I in these two stages of the reaction pathway and allow detailed analysis of the roles of active site residues in catalysis. The active site geometry of the Tyr146Phe FBPA variant with the carbinolamine intermediate supports the notion that in the archaeal FBPA I Tyr146 is the proton donor catalyzing the conversion between the carbinolamine and Schiff base. Our structural analysis furthermore indicates that Glu187 is the proton donor in the eukaryotic FBPA I, whereas an aspartic acid, conserved in all FBPA I enzymes, is in a perfect position to be the general base facilitating carbon−carbon cleavage. The crystal structure of the Trp144Glu, Tyr146Phe double-mutant substrate complex represents the first example where the cyclic form of β-fructose 1,6-bisphosphate is noncovalently bound to FBPA I. The structure thus allows for the first time the catalytic mechanism of ring opening to be unraveled.

Fructose-1,6-bisphosphate aldolase (FBPA,[1] EC 4.1.2.13) catalyzes the reversible formation of fructose 1,6-bisphosphate (FBP) from glyceraldehyde 3-phosphate (GAP) and dihydroxyacetone phosphate (DHAP). FBPA is an essential enzyme in the reversible Embden−Meyerhof−Parnas pathway and the Calvin cycle. Two classes of FBPAs, which differ with respect to reaction mechanism and distribution in the biosphere, have been identified (*1*). Class I FBPA (FBPA I) utilizes a Schiff base reaction mechanism and was originally found in animals, plants, protozoans, and algae (*2*) but has also been identified in bacteria and archaea (*3*, *4*). FBPA II uses divalent metal ions for catalysis and has been found in bacteria and fungi (*5*).

FBPA I is grouped into two different sequence families, one with only eukaryotic members and one with both bacterial and archaeal members (termed the archaeal FBPA I or FBPA IA) (*6*). Several crystal structures have shown that the eukaryotic FBPA I is a homotetramer, where the subunits adopt the fold of a parallel $(\beta\alpha)_8$-(TIM)-barrel (*7*−*9*). Although the archaeal FBPA I subunit also displays the $(\beta\alpha)_8$-barrel fold, its quaternary structure is that of a homodecamer resulting from the dimerization of two identical pentamers (*10*). The two types of FBPA I enzymes are, despite the lack of any significant overall sequence identity, clearly homologous as seen from the many active site residues conserved with respect to sequence, structure, and function (*10*, *11*). Together with the similar binding modes for Schiff base intermediates of the substrate DHAP, this strongly indicates a similar catalytic mechanism for the eukaryotic and the archaeal FBPA I.

Aldolases catalyze the formation and cleavage of a C−C bond between a wide variety of substrates and have for this reason been given considerable attention as possible biocatalysts (*12*). Although it is known that the FBPA I reaction mechanism proceeds via a number of intermediates covalently bound to the catalytic lysine, it is still a matter of debate how the efficient conversion between intermediates is facilitated. This is partly due to the fact that only the crystal structure of the Schiff base intermediate of DHAP has so far been solved (*10*, *13*). FBPA I only utilizes the cyclic form of the β-anomer of the substrate (β-FBP), and the initial step of the reaction mechanism is ring opening to produce acyclic FBP (*14*). However, the residues catalyzing this step are unknown. So far three crystal structures of eukaryotic FBPA I in noncovalent complexes with the substrates FBP

‡ Data deposition: The crystal structures and the X-ray diffraction data have been deposited into the Protein Data Bank with the accession codes 1W8R and 1W8S.

* To whom correspondence should be addressed. Current address: Swiss Light Source at Paul Scherrer Institut, CH-5232 Villigen, Switzerland. Phone: 0041-56-310-5177. Fax: 0041-56-310-3151. E-mail: Ehmke.pohl@psi.ch.

§ European Molecular Biology Laboratory.

|| University of Duisburg-Essen.

[1] Abbreviations: FBPA, fructose-1,6-bisphosphate aldolase; TIM, triose phosphate isomerase; FBP, fructose 1,6-bisphosphate; GAP, glyceraldehyde 3-phosphate; DHAP, dihydroxyacetone phosphate; rms, root mean square; Tt, *Thermoproteas tenax*.

10.1021/bi048192o CCC: $30.25
Published on Web 02/17/2005

and DHAP have been determined but show inconsistent binding modes. Where one structure has the substrate FBP bound in a position clearly incompatible with catalysis (*15*), another study identified three different binding sites for DHAP and suggested that they represent a trajectory for product exchange (*16*). A third study identified FBP in a favorable position for catalysis and positively located the substrate-binding residues (*17*). Following the ring opening is the nucleophilic attack of a lysine on the carbonyl group of the substrate, which leads to the formation of the covalent carbinolamine intermediate (*18*, *19*). Subsequently, a proton is donated to the carbinolamine followed by dehydration to yield the Schiff base. Another proton is then subtracted from the 4′-hydroxyl, leading to C3−C4 breakage and release of the product GAP. However, it is still controversial which residue serves as the acid mediating Schiff base formation and which as the base mediating C3−C4 cleavage. It was suggested on the basis of the crystal structure of a Schiff base intermediate that Glu187 could be the acid (*13*). Contrary to this, Glu187 was in an enzymatic study of mutant FBPA I proposed to promote Schiff base formation and to act as the general base (*20*). Also Asp33, which was identified as an essential catalytic residue (*21*), has been proposed as a likely candidate for the general base leading to C3−C4 cleavage (*13*).

To gain a more complete understanding of the catalytic mechanism of an enzyme, one would ideally, in addition to detailed enzymological studies, determine crystal structures of every intermediate along the reaction path (*22*). This is unfortunately hampered by the difficulty of trapping transient intermediates. In this paper, we present a catalytically deficient FBPA IA mutant (Tyr146Phe) from the hyperthermophilic archaeal organism *Thermoproteus tenax*. The mutant enzyme allowed us to solve the crystal structure of a trapped covalently bound carbinolamine intermediate. A second FBPA IA double variant (Trp144Glu, Tyr146Phe) facilitated the crystal structure of the enzyme in complex with the cyclic form of the substrate β-FBP. These crystal structures are the first to be solved of these two steps along the reaction path and provide novel insights into the catalytic mechanism of the Schiff base forming FBPA.

MATERIALS AND METHODS

Site-Directed Mutagenesis. The point mutations were constructed according to the modified procedure of the Stratagene QuickChange protocol (*23*). The mutations were introduced using 5′-phosphorylated anti-sense primers (introduced mutations shown in bold):

Tyr146Phe: 5′-CTTTCCCGCCCCT**T**GGG**A**ACG
ACCAGACCACCAG-3′

Tyr146Phe, Trp144Glu:
5′-GGGAACGAC**TC**GACCACCAGGGGC-3′

For the Tyr146Phe substitution, a silent mutation was introduced to remove an *Ava*I restriction site. The double mutant was constructed from the plasmid of the already obtained single mutant using the above primer. The mutations were confirmed by sequencing in both directions, and the proteins were expressed and purified using the same procedures as for the native protein.

Enzymatic Assays. Enzymatic activity of the mutant proteins was measured in a coupled assay at 50 °C as described previously (*6*). Up to 200 μg of mutant protein was tested in 1 mL of 100 mM Tris−HCl (pH 7.0 at 50 °C) containing 10 mM FBP and 0.4 mM NADH as well as the auxiliary enzymes triose phosphate isomerase and glycerol-3-phosphate dehydrogenase. Commercially available rabbit FBPA I and recombinant wild-type FBPA IA from *T. tenax* were used as controls.

Crystallization and Data Collection. Both FBPA variants were concentrated to 8 mg/mL as determined by the Bradford assay (*24*) and crystallized as previously described (*10*). Monoclinic crystals were soaked for 2 min in the cryobuffer (mother liquor plus 20% glycerol) containing a 100 mM concentration of the substrate FBP. The crystals were mounted in nylon loops (*25*), and X-ray diffraction data were collected at 100 K from monoclinic crystals on the EMBL beam lines BW7B (*26*) and X11 (*27*) located at the DORISIII storage ring at DESY. All diffraction data were integrated and scaled using DENZO and SCALEPACK (*28*).

Structure Solution and Refinement. The model of the native protein (PDB code 1OJX) was used as a starting point for solving the mutant protein crystal structures. Initially, the structures were refined with each subunit as a rigid body followed by restrained refinement of coordinates as well as temperature factors using bulk solvent correction and anisotropic scaling and with each monomer defined as a TLS group in the program REFMAC (*43*). The structures were refined without noncrystallographic symmetry restraints as this gave a lower R_{free} value. Bound substrates were identified and built in unbiased σ_A-weighted $F_o - F_c$ and $2F_o - F_c$ electron density maps (*29*) using the interactive graphics program XtalView (*30*). After several rounds of iterative model building in XtalView and restrained refinement in REFMAC, waters were added in an automated manner by the ARP/wARP 6.0 program (*31*). Further details are summarized in Table 1. Comparisons and superpositions of active sites were carried out using the graphics program O (*32*). Figures 1−5 were made with MOLSCRIPT (*33*) and BOBSCRIPT (*34*).

RESULTS AND DISCUSSION

Enzymatic Activity of the Active Site Variants: Tyr146 of Tt FBPA IA Is an Essential Catalytic Residue. On the basis of structural comparisons, Tyr146 of the archaeal FBPA I was predicted to be important for catalysis as its side chain hydroxyl occupies a position equivalent to that of the carboxyl of the catalytically vital Glu187 of the eukaryotic FBPA I (*10*). The Tyr146Phe point mutation was constructed to evaluate the importance of the hydroxyl of the tyrosine in catalysis. The mutant protein was folded and soluble as it behaved identically to the native enzyme in size exclusion chromatography as well as in our crystallization experiments. Enzyme assays revealed that the catalytic rate of the mutant protein is at least 3 orders of magnitude lower than for the native *T. tenax* FBPA IA. These results clearly demonstrate that Tyr146 is an essential residue in the catalysis of FBPA IA from *T. tenax*. To investigate if the glutamic acid important for catalysis in eukaryotic FBPA I (Glu187 of human FBPA I) could restore the lost activity of the Tyr146Phe mutant of the archaeal FBPA I, the Trp144Glu,

Table 1: Summary of the X-ray Data Collection and Refinement Statistics

	Tyr146Phe carbinolamine intermediate	Trp144Glu, Tyr146Phe cyclic β-FBP complex
space group	$P2_1$	$P2_1$
cell dimensions *a*, *b*, *c* (Å); β (deg)	82.9, 159.2, 101.4; 107.8	82.5, 157.3, 101.2; 107.9
wavelength (Å)	0.812	0.842
resolution (Å)	40−1.93	40−1.85
$I/\sigma(I)^a$	16.2 (2.2)	22.0 (2.2)
$R_{merge}{}^{a,b}$	0.079 (0.368)	0.057 (0.328)
completeness[a]	0.973 (0.776)	0.955(0.629)
no. of reflns in working set	179009	197604
no. of reflns in test set	2723	2012
no. of protein residues	2502	2502
$R_{cryst}{}^c$	0.148	0.149
R_{free}	0.187	0.187
RMSD(bonds)[d] (Å)	0.014	0.014
RMSD(angles)[d] (deg)	1.5	1.5

[a] The numbers in parentheses correspond to the last resolution shell. [b] $R_{merge} = \sum_{hkl}\sum_i|I(hkl) - \langle I(hkl)\rangle|/\sum_{hkl}\sum_i I(hkl)$. [c] $R_{cryst} = \sum_{hkl}||F_o(hkl)| - k|F_c(hkl)||/\sum_{hkl}|F_o(hkl)|$. [d] Root-mean-square deviations from ideal values.

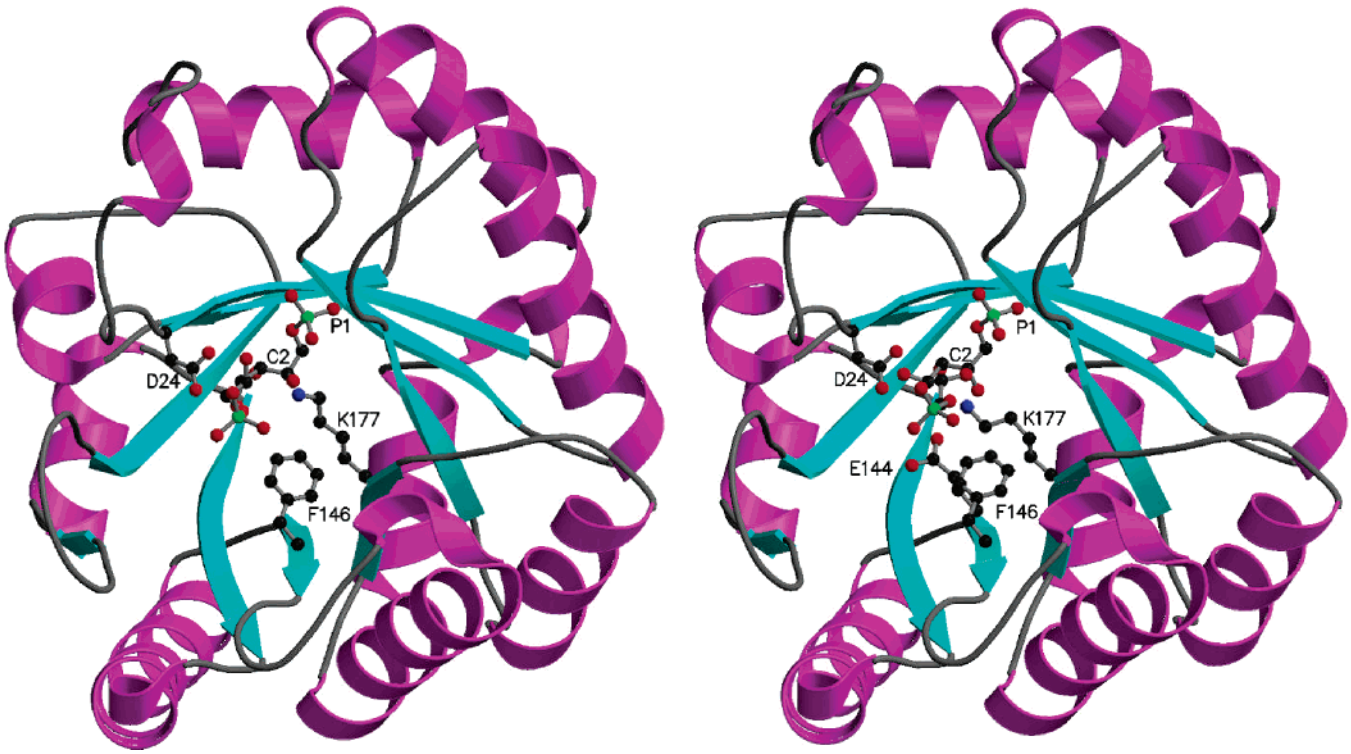

FIGURE 1: (a, left) Ribbon diagram of the crystal structure of the Tyr146Phe *T. tenax* FBPA monomer in complex with FBP. The C-terminal side with the mutated residue and the covalently linked intermediate is shown in a ball-and-stick model. (b, right) Ribbon diagram of the Trp144Glu, Tyr146Phe double-mutant *T. tenax* FBPA IA monomer in the same orientation. The substrate β-FBP, the Schiff base forming Lys177, and the introduced residues Glu144 and Phe146 are shown in a ball-and-stick representation.

Tyr146Phe double mutant was constructed and the mutant protein expressed and purified. The Trp144Glu, Tyr146Phe double mutant was correctly folded and soluble but did not display any detectable catalytic activity.

Crystal Structures of Substrate-Bound Complexes. To obtain detailed molecular insights into the catalysis of the Schiff base forming FBPA, we determined the crystal structures of the *T. tenax* Tyr146Phe (Figure 1a) and Trp144Glu, Tyr146Phe FBPA IA (Figure 1b) in complex with the substrate FBP at resolutions of 1.9 Å. Crystals of the mutant enzymes are isomorphous to the monoclinic crystals of the native enzyme described previously (*10*) and also contain one decamer in the asymmetric unit. The mutations do not cause any larger overall structural changes, and the mutant protein structures superimpose very well with rms deviations between Cα traces of 0.1−0.3 Å with the structures of the native protein. The two structures presented here yielded R_{free} values (*35*) of 19% and are of excellent quality with more than 94% of the residues in the most favored region and no residues in the generous or disallowed regions of the Ramachandran plot (see Table 1 for more data collection and refinement statistics) (*36*).

For both the Tyr146Phe and the Trp144Glu, Tyr146Phe mutant enzymes, unbiased σ_A-weighted electron density maps (*29*) unambiguously showed that the substrate FBP is bound in the active sites of all 10 subunits of the decamer. However, it is clear from the electron density maps that the substrate is bound as different chemical forms in the two cases. In the case of the single-point mutant, continuous electron density from the catalytic lysine to the substrate shows that

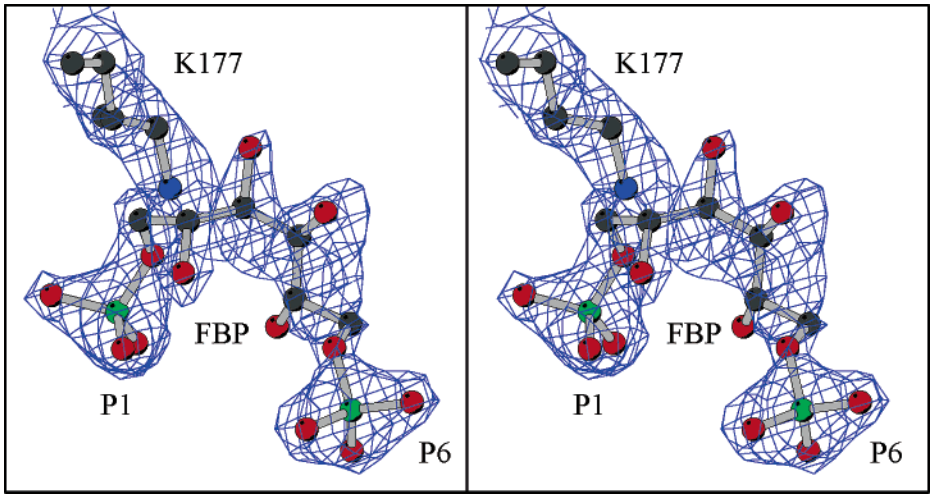

FIGURE 2: Stereoview of the unbiased $2F_o - F_c$ electron density contoured at 1σ around the active site of the Tyr146Phe mutant of FBPA IA from *T. tenax*. The carbinolamine intermediate of the substrate FBP and the lysine covalently bound to the substrate are shown in a ball-and-stick representation. To avoid any model bias, both electron density maps displayed in Figures 2 and 3, respectively, were calculated using phases from a model prior to adding the bound substrates. The *B* factors of the covalently bound intermediate range from 9 to 30 Å^2 in the 10 crystallographically independent subunits. These values compare well with those of the atoms of surrounding residues (9−25 Å^2), indicating similar occupancies. The conserved binding pocket P1−C4 binds with higher affinity than C5−P6 as reflected by higher *B* factors and weaker electron density.

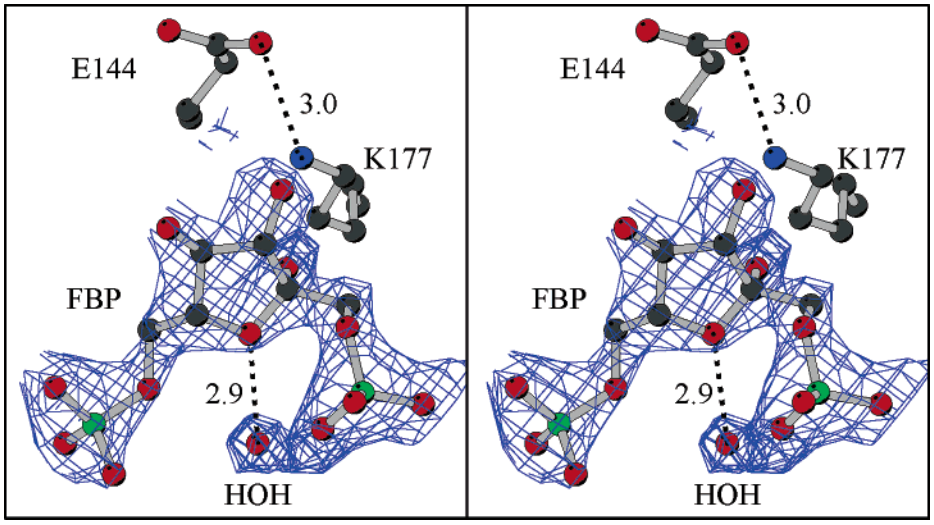

FIGURE 3: Stereoview of the unbiased $F_o - F_c$ electron density contoured at 3σ around the active site of the Trp144Glu, Tyr146Phe double mutant of FBPA IA from *T. tenax*. The substrate β-FBP, bound noncovalently in its cyclic form, the active site lysine, and the introduced Glu144 are shown in ball-and-stick representation. Numbers for distances between atoms are shown in Å.

a covalently bound intermediate is trapped in the crystal (Figure 2). The active site lysine (Lys177 in *T. tenax* FBPA IA) has thus already completed the nucleophilic attack on the carbonyl (C2) of the substrate. Because of the relatively high resolution of the data, the C2 of the substrate is clearly seen to have a non-hydrogen atom bound covalently. The crystal structure is thus of an intermediate prior to dehydration of O2 and Schiff base formation. This structure most likely represents the carbinolamine intermediate, where a hydroxyl is bound to the C2 atom of the substrate adduct. This is further supported by the tetrahedral nature of the electron density around C2 (Figure 2). In the case of the Trp144Glu, Tyr146Phe double-mutant protein crystal, the electron density is discontinuous between the catalytic lysine and the substrate, which identifies the complex as noncovalent (Figure 3). Furthermore, β-FBP is clearly bound as the cyclic form as seen from the pentagonal character of the electron density.

It is important to note that the native protein shows high catalytic activity under the crystallization conditions (data not shown). Furthermore, as the crystal structures presented here were obtained by soaking experiments, the variant proteins are active in their crystalline state to the point of the trapped intermediate. Therefore, the crystal structures represent catalytically competent conformers of the enzyme.

Schiff Base Formation Is Catalyzed by a Tyrosine in Most Archaeal FBPA I Enzymes and by a Glutamic Acid in Eukaryotic FBPA I. We have managed to trap and solve the crystal structure of the carbinolamine intermediate of a Tyr146Phe mutant of an archaeal FBPA I. The Tyr146Phe mutation does not induce significant structural changes in the active site, and the catalytic residues occupy positions identical to those seen in previously solved crystal structures of wild-type FBPAs (Figure 4) (*10*). Furthermore, the aromatic ring of Phe146 occupies a position similar to that of the aromatic ring of Tyr146. This result provides strong

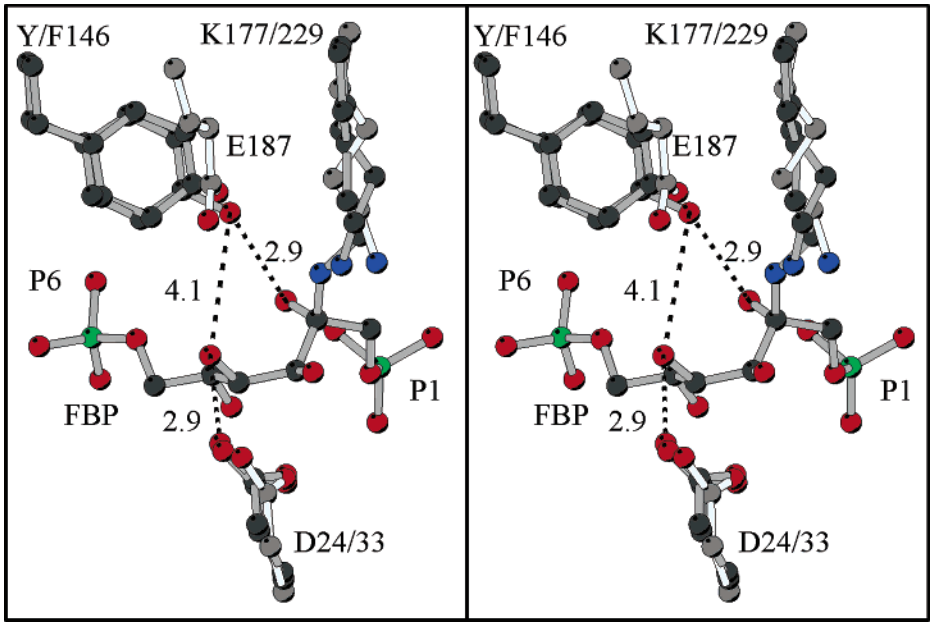

FIGURE 4: Stereoview of the active sites of the *T. tenax* native FBPA IA (PDB code 1OJX) and Tyr146Phe mutant FBPA IA (gray bonds) as well as native human FBPA I (PDB code 4ALD, white bonds) after the equivalent atoms of the six active site residues that are structurally conserved between the eukaryotic and the archaeal FBPA (Ala22, Asp24, Lys177, Gly204, Gly231, and Arg233) have been superimposed by least-squares techniques. The resulting rms deviation is 1.1 Å. Important active site residues and the carbinolamine of the substrate FBP are shown in ball-and-stick representation. Residues Y/F146, K177, and D24 correspond to the *T. tenax* FBPA IA, whereas K229, E187, and D33 match the human FBPA I. The distances between atoms are given in Å.

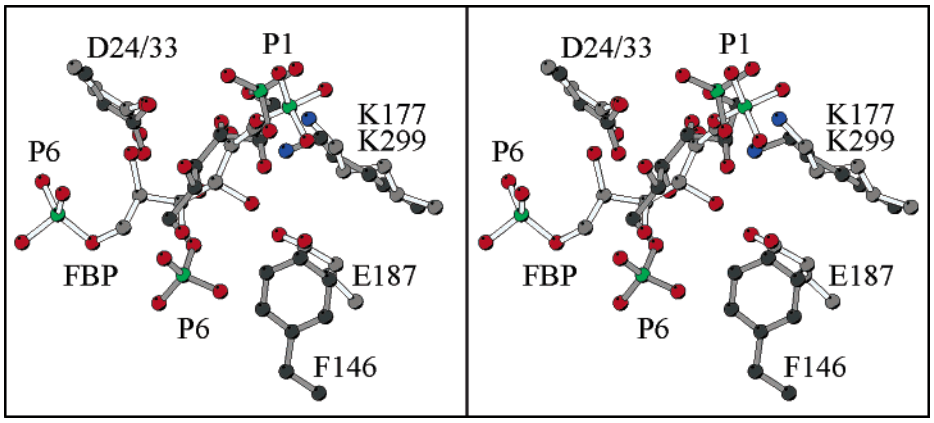

FIGURE 5: Stereoview of the different binding modes of noncovalently bound FBP in human FBPA I (PDB code 4ALD, white bonds) and the covalently bound carbinolamine intermediate of the Tyr146Phe FBPA IA of *T. tenax* (dark bonds). The phosphates with equivalent and with different binding sites are labeled P1 (DHAP phosphate) and P6 (GAP phosphate), respectively.

evidence that Tyr146 of *T. tenax* FBPA IA is important in the catalytic step where the carbinolamine is converted into the Schiff base. The deficiency in Schiff base formation is not a result of the specific crystallization conditions as a Schiff base intermediate was trapped in crystals of the native protein grown under identical conditions (*10*). The comparison of the active sites of native and mutant protein structures shows that Tyr146 would be in a perfect position to act as proton donor as its hydroxyl would be only 2.9 Å from the proton-accepting hydroxyl at C2 of the substrate intermediate (Figure 4). The hydroxyl of Tyr146 would be 4.1 Å from the C4 hydroxyl of the substrate, and it is therefore implausible that it plays a role as the general base in C3−C4 cleavage. We can therefore conclude that Tyr146 is the proton donor facilitating the efficient dehydration of the carbinolamine, leading to the Schiff base in FBPA IA of *T. tenax*. Twenty of the 27 genes identified to date as encoding archaeal FBPA I have Tyr146 conserved, and it is likely that the tyrosine serves the same catalytic function as proton donor in these enzymes. Of the seven FBPA IA lacking the tyrosine, two have the glutamic acid that serves as a proton donor in the eukaryotic FBPA I (see the following sections). In the five genes missing both Tyr146 and Glu187 the residue corresponding to Tyr146 in *T. tenax* is Thr, Gly, or Ala. None of these residues can apparently act as a proton donor. Thus, yet another residue has to fulfill this role in catalysis.

The high degree of conservation of active site residues and the similar binding modes of Schiff base intermediates of DHAP published previously indicate similar catalytic pathways for the eukaryotic and the archaeal FBPA I (*10*). The comparison of the structure of the carbinolamine intermediate of FBP presented here with the structure of a human FBPA I in a noncovalent complex with FBP in its linear form (*17*) is shown in Figure 5. Here, the P1 (DHAP) phosphate is seen to bind in a similar manner by residues preceding β-strands 7 and 8, which represents a common

phosphate binding site found in many enzymes of the $(\beta\alpha)_8$-barrel fold utilizing phosphorylated substrates (*37*). The part of the substrates between carbon atoms C1 and C4 also binds in a similar way, whereas the part from C5 to the second phosphate (P6, GAP) binds differently in the eukaryotic and the archaeal FBPA I. Different binding pockets position the P6 phosphates 5.4 Å apart (Figure 5). This result may indicate that the binding pocket for the P6 phosphate was not present in a common ancestor protein, but has later evolved in different ways. However, the different binding pockets for the P6 phosphate do not count against the notion of a similar reaction mechanism as only the central part (C2−C4) of the substrate is chemically altered along the reaction path (*13*).

A glutamic acid (Glu187 in human FBPA I) is completely conserved in the active site of all eukaryotic FBPA I enzymes studied to date. Glu187 was shown to be catalytically essential as the mutation to glutamine results in a 3 orders of magnitude lower catalytic rate (*20*). Two different catalytic roles have been proposed for Glu187. A recent biochemical study of Glu187 mutants concluded that this residue fulfills a multiple role in mammalian aldolases including Schiff base formation and C3−C4 cleavage (*20*). Another study, based on the crystal structure of a Schiff base intermediate of DHAP, concluded that Glu187 serves as the acid facilitating the dehydration of the carbinolamine (*13*). From the structural superposition of human and *T. tenax* FBPA IA, it is clear that the carboxyl of Glu187 (human FBPA I) occupies a position very similar to that of the hydroxyl of Tyr146 (*T. tenax* FBPA IA) (Figure 4). This indicates, in agreement with Choi et al. (*13*), that Glu187 is indeed the proton donor converting the carbinolamine into the Schiff base in the eukaryotic FBPA I.

A Conserved Aspartic Acid Is the General Base in FBPA I/IA. An important step in the catalytic mechanism of FBPA I is the proton subtraction from the C4 hydroxyl of FBP, leading to breakage of the C3−C4 bond. The three residues Asp33, Lys146, and Glu187 have all been suggested to be the general base for this step. The carboxyl moiety of Glu187 of the eukaryotic FBPA I is located at the same position as the hydroxyl of Tyr146 of *T. tenax* FBPA IA, but as both would be more than 4 Å from the hydroxyl at C4 of the carbinolamine intermediate, it is not likely that these residues serve the role as the general base (Figure 4).

Lys146 is located at the end of β-strand 4 in all eukaryotic FBPA I enzymes and was from biochemical investigations proposed to be the general base in FBPA I (*38*). However, modeling the C4−O4 in the Schiff base intermediate of DHAP placed the Nϵ atom of Lys146 almost 6 Å from the O4 hydroxyl (*13*). Lys146 is not conserved in the sequence of any archaeal FBPA I. Lys78 is in FBPA IA from *T. tenax* located at the end of β3 and has its Nϵ 4.4 Å from the Nϵ of Lys146 in the eukaryotic FBPA I and could be functionally equivalent. However, the Nϵ of Lys78 is 5.4 Å from the O4 hydroxyl of the carbinolamine intermediate, and it is highly improbable that it serves the function as the general base. However, one aspartic acid is completely conserved in all eukaryotic and archaeal FBPA I sequences identified so far (Asp24 in FBPA IA from *T. tenax* and Asp33 in human FBPA I). Asp33 was in a mutagenesis study identified as an important catalytic residue (*21*) and was on the basis of structure-based modeling proposed to be the general base responsible for C3−C4 cleavage (*13*). The aspartic acids occupy structurally equivalent positions in the archaeal and the eukaryotic FBPA I and are thus likely to serve identical functions in catalysis. In the crystal structure of the carbinolamine intermediate presented here, the carboxyl of the aspartic acid is located 2.9 Å from the O4 hydroxyl of the carbinolamine intermediate and is thus in a perfect position to be the general base mediating C3−C4 cleavage (Figure 4). Furthermore, the residue adopts the same conformation in the crystal structure of Tt-FPBA in the Schiff base intermediate with the substrate DHAP published previously by Lorentzen et al. (*10*). As this aspartic acid is completely conserved with respect to sequence and structure in all FBPA I/Ia enzymes studied so far, it seems likely that it serves as a base in all members of this enzyme family. The catalytic mechanism would thus be different from the one suggested for the D-2-deoxyribose-5-phosphate aldolase where an activated water molecule has been suggested to be involved in substrate deprotonation (*22*). However, as long as the genuine Schiff base intermediate with FBP has not been trapped in a crystal structure, we cannot rule out the possibility that dehydration of O2 leads to a conformational change that prevents Asp 33 from taking part in the next step of catalysis.

Crystal Structure of a Cyclic FBP Complex and the Mechanism of Ring Opening. The Trp144Glu, Tyr146Phe double mutant of *T. tenax* FBPA IA was originally constructed to test whether Glu144 can functionally replace Tyr146. In the native structure the side chain of Trp144 adopts a conformation where a simple substitution by a glutamate would bring the carboxyl moiety into a position favorable for catalysis. However, no catalytic activity could be detected of this double mutant. The crystal structure of the Trp144Glu, Tyr146Phe variant in complex with the cyclic form of the substrate β-FBP shows that perturbation of several active site residues explains the lack of activity of the double-mutant enzyme (Figure 3). The side chain of the newly introduced Glu144 adopts a conformation very different from that seen in crystal structures of eukaryotic FBPA I. The carboxyl group of Glu144 is located too far from the substrate (more than 5 Å from the C2 hydroxyl of the substrate) to participate in catalysis. The different conformations of the glutamic acid side chains are the results of different local environments in the active sites of *T. tenax* FBPA IA and eukaryotic FBPA I. In FBPA I, the side chain of the conserved Lys146 sterically blocks for the alternative conformation of the glutamic acid seen in *T. tenax* FBPA IA. *T. tenax* FBPA IA has a glycine (Gly110) at the position of Lys146, and 25 of the 27 FBPA IA proteins have one of the small residues glycine, alanine, or serine at this position. The two FBPA IA proteins with the catalytic glutamate both have larger residues (valine or leucine) at the Lys146 position, and these residues probably serve to keep the glutamate in the correct position for catalysis. In *T. tenax* FBPA IA, the side chain of the Schiff base forming Lys177 furthermore moves by 1.5 Å and adopts a new conformation in which it forms a salt bridge with Glu144. The lack of activity of the Trp144Glu, Tyr146Phe mutant enzyme is therefore due to the local structural differences of the active sites of the eukaryotic and the archaeal FBPA I, which do not allow Glu144 and Lys177 to adopt the conformations needed for efficient catalysis.

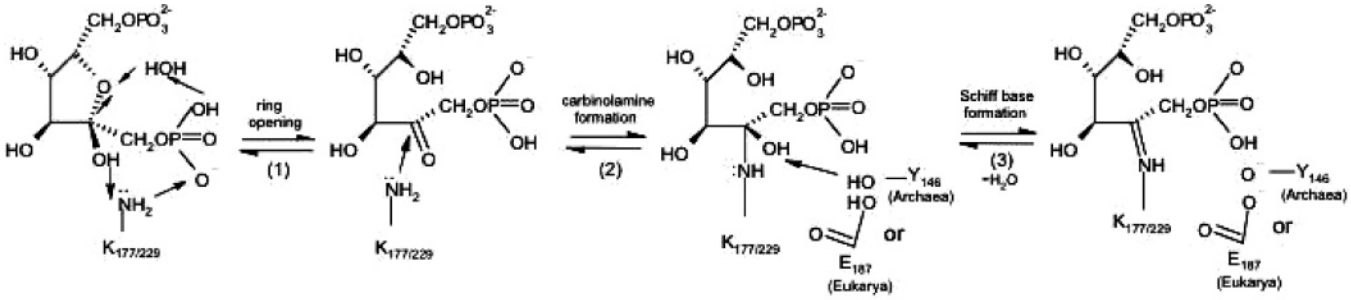

FIGURE 6: Proposed reaction mechanism for the first three catalytic steps leading to the Schiff base intermediate for class I/IA FBPA. The H_2O participating in ring opening (step 1) is not seen in the crystal structures of the carbinolamine or Schiff base intermediates and is probably displaced to the solvent after ring opening. Schiff base formation (step 3) is in the case of the eukaryotic FBPA I catalyzed by Glu187 and in the case of most archaeal FBPA I by Tyr146.

It is highly remarkable that the cyclic form of the substrate is bound in the active site of the Trp144Glu, Tyr146Phe mutant protein. This result shows that the double-mutant enzyme is impaired in the ring-opening mechanism of the substrate β-FBP. FBP exists in solution in equilibrium between α- and β-anomers (ratio of approximately 20:80) with only a small percentage on the acyclic keto form (*39*). It has for a long time been an unresolved question whether FBPA I utilizes the cyclic or the acyclic form (or both) of the substrate (*40*). As FBP predominantly exists as the cyclic form in solution, it was suggested that the cyclic form initially binds in the active site and is then converted into the acyclic form by the enzyme (*41*, *42*). A recent study used transient-state kinetics in single-turnover experiments to demonstrate that FBPA I only utilizes cyclic β-FBP as a substrate and that ring opening is indeed catalyzed by the enzyme (*14*). However, the residues involved in ring opening are unknown. The crystal structure of the Trp144Glu, Tyr146Phe mutant *T. tenax* FBPA IA in complex with cyclic β-FBP allows us for the first time to explore the mechanism of ring opening. Conversion of cyclic FBP into the acyclic keto form requires proton donation to the bridging oxygen (O5) and proton removal from the 2′ hydroxyl (Figure 6). In the structure with β-FBP bound, a water molecule is seen to be in a perfect position to facilitate proton transfer to O5 (Figure 3). The water is coordinated by the backbone NH of Gly204, a P1 phosphate oxygen of β-FBP, and the side chain of Ser202 and is positioned 2.9 Å from O5 of the substrate in all 10 subunits of the enzyme. This water molecule is not present in the crystal structures of the apo form of native Tt-FBPA or in the carbinolamine or Schiff base intermediates but appears to be bound only in conjunction with cyclic β-FBP. The most likely candidate for the base removing a proton from 2′-OH of the substrate is the Schiff base forming lysine. In the structure of the wild-type FBPA IA the pK_a of the catalytic lysine could be reduced by the close proximity to the nitrogen atom of Trp144. The Nϵ atom of Lys177 is 2.6 Å from 2′-OH in the Trp144Glu, Tyr146Phe mutant *T. tenax* FBPA IA and is thus close enough to be the base. In the crystal structure of the native Tt-FBPA IA the Nϵ atom of Lys177 would be only 1.7 Å from the 2-OH of the substrate. The close proximity may suggest that ring opening occurs simultaneously with substrate binding. Lys177 is in the double variant seen to form a salt bridge to Glu144 and thus kept in a protonated state, which explains why ring opening is impaired in this mutant protein. After ring opening, Lys177 would need to be deprotonated to make the nucleophilic attack on the carbonyl group of the substrate. There is no conserved residue in a favorable position to perform the deprotonation of Lys177, but it is possible that the proton is transferred to the solvent via the P1 phosphate (Figure 6). As the positions of the Schiff base forming lysine and of Gly204 as well as the P1 phosphate are conserved between the archaeal and the eukaryotic FBPA I, the ring-opening mechanism involving an activated water and the Schiff base forming lysine proposed here could be common to all FBPA I/IA.

CONCLUSION

We have here presented two catalytically deficient active site variants of the Schiff base forming fructose-1,6-bisphosphate aldolase from the hyperthermophilic archaeal organism *T. tenax*. The mutant proteins were designed to gain further insight into the catalytic mechanism of class I FBPAs. The two high-resolution crystal structures of protein−substrate complexes, presented here, represent different states along the reaction path. These structures elucidate the poorly understood early steps of the catalytic mechanism of this class of enzymes. The Tyr146Phe mutant allowed us to determine the crystal structure of a trapped covalently bound carbinolamine of the substrate fructose-1,6-bisphosphate. The active site geometry observed in this crystal structure supports the notion of a catalytic mechanism where the proton donor necessary for the conversion of the carbinolamine into the Schiff base is Tyr146 in most archaeal and Glu187 in all eukaryotic fructose-1,6-bisphosphate aldolases. A completely conserved aspartic acid on the other hand is in a perfect position to be the base mediating carbon−carbon cleavage in the archaeal as well as the eukaryotic fructose-1,6-bisphosphate aldolase. Additionally, an enzymatically deficient double mutant (Tyr146Phe, Trp144Glu) facilitated the first crystal structure of this enzyme family in complex with the cyclic form of the substrate fructose 1,6-bisphosphate. The enzyme-catalyzed mechanism of ring opening can most likely be ascribed to the Schiff base forming lysine and a well-ordered water molecule. The analysis of the two new crystal structures presented here has thus led to a more complete understanding of the mechanism of catalysis for class I fructose-1,6-bisphosphate aldolases.

ACKNOWLEDGMENT

We are very grateful to Anna Peyker and Dorothea Schuette for excellent help with constructing point mutations and many valuable discussions.

REFERENCES

1. Rutter, W. J. (1964) Evolution of aldolase, *Fed. Proc. 23*, 1248−1257.
2. Rutter, W. J., and Groves, W. E. (1964) *Taxonomic biochemistry and serology*, Vol. 417, N. Y. Ronald Press, New York.
3. Thomson, G. J., Howlett, G. J., Ashcroft, A. E., and Berry, A. (1998) The dhnA gene of Escherichia coli encodes a class I fructose bisphosphate aldolase, *Biochem. J. 331*, 437−45.
4. Galperin, M. Y., Aravind, L., and Koonin, E. V. (2000) Aldolases of the DhnA family: a possible solution to the problem of pentose and hexose biosynthesis in archaea, *FEMS Microbiol. Lett. 183*, 259−64.
5. Lebherz, H. G., and Rutter, W. J. (1969) Distribution of fructose diphosphate aldolase variants in biological systems, *Biochemistry 8*, 109−21.
6. Siebers, B., Brinkmann, H., Dorr, C., Tjaden, B., Lilie, H., van der Oost, J., and Verhees, C. H. (2001) Archaeal fructose-1,6-bisphosphate aldolases constitute a new family of archaeal type class I aldolase, *J. Biol. Chem. 276*, 28710−8.
7. Gamblin, S. J., Cooper, B., Millar, J. R., Davies, G. J., Littlechild, J. A., and Watson, H. C. (1990) The crystal structure of human muscle aldolase at 3.0 Å resolution, *FEBS Lett. 262*, 282−6.
8. Hester, G., Brenner-Holzach, O., Rossi, F. A., Struck-Donatz, M., Winterhalter, K. H., Smit, J. D., and Piontek, K. (1991) The crystal structure of fructose-1,6-bisphosphate aldolase from Drosophila melanogaster at 2.5 Å resolution, *FEBS Lett. 292*, 237−42.
9. Sygusch, J., Beaudry, D., and Allaire, M. (1987) Molecular architecture of rabbit skeletal muscle aldolase at 2.7-A resolution, *Proc. Natl. Acad. Sci. U.S.A. 84*, 7846−50.
10. Lorentzen, E., Pohl, E., Zwart, P., Stark, A., Russell, R. B., Knura, T., Hensel, R., and Siebers, B. (2003) Crystal structure of an archaeal class I aldolase and the evolution of $(\beta/\alpha)_8$ barrel proteins, *J. Biol. Chem. 278*, 47253−47260.
11. Lorentzen, E., Siebers, B., Hensel, R., and Pohl, E. (2004) Structure, function and evolution of the Archaeal class I fructose-1,6-bisphosphate aldolase, *Biochem. Soc. Trans. 32*, 259−63.
12. von der Osten, C. H., Gioannetti, C., Barbas, C., Pederson, R. L., Wang, Y. F., Wong, C. H., Ozaki, A., Toone, E., Whitesides, G. M., and Sinskey, A. J. (1990) Molecular cloning of aldolases for synthetic applications, *Ann. N. Y. Acad. Sci. 613*, 771−5.
13. Choi, K. H., Shi, J., Hopkins, C. E., Tolan, D. R., and Allen, K. N. (2001) Snapshots of catalysis: the structure of fructose-1,6-(bis)phosphate aldolase covalently bound to the substrate dihydroxyacetone phosphate, *Biochemistry 40*, 13868−75.
14. Choi, K. H., and Tolan, D. R. (2004) Presteady-state kinetic evidence for a ring-opening activity in fructose-1,6-(bis)phosphate aldolase, *J. Am. Chem. Soc. 126*, 3402−3.
15. Choi, K. H., Mazurkie, A. S., Morris, A. J., Utheza, D., Tolan, D. R., and Allen, K. N. (1999) Structure of a fructose-1,6-bis-(phosphate) aldolase liganded to its natural substrate in a cleavage-defective mutant at 2.3 Å, *Biochemistry 38*, 12655−64.
16. Blom, N., and Sygusch, J. (1997) Product binding and role of the C-terminal region in class I D-fructose 1,6-bisphosphate aldolase, *Nat. Struct. Biol. 4*, 36−9.
17. Dalby, A., Dauter, Z., and Littlechild, J. A. (1999) Crystal structure of human muscle aldolase complexed with fructose 1,6-bisphosphate: mechanistic implications, *Protein Sci. 8*, 291−7.
18. Rose, I. A., Warms, J. V., and Kuo, D. J. (1987) Concentration and partitioning of intermediates in the fructose bisphosphate aldolase reaction. Comparison of the muscle and liver enzymes, *J. Biol. Chem. 262*, 692−701.
19. Rose, I. A., and Warms, J. V. (1985) Complexes of muscle aldolase in equilibrium with fructose 1,6-bisphosphate, *Biochemistry 24*, 3952−7.
20. Maurady, A., Zdanov, A., de Moissac, D., Beaudry, D., and Sygusch, J. (2002) A conserved glutamate residue exhibits multifunctional catalytic roles in D-fructose-1,6-bisphosphate aldolases, *J. Biol. Chem. 277*, 9474−83.
21. Morris, A. J., and Tolan, D. R. (1993) Site-directed mutagenesis identifies aspartate 33 as a previously unidentified critical residue in the catalytic mechanism of rabbit aldolase A, *J. Biol. Chem. 268*, 1095−100.
22. Heine, A., DeSantis, G., Luz, J. G., Mitchell, M., Wong, C. H., and Wilson, I. A. (2001) Observation of covalent intermediates in an enzyme mechanism at atomic resolution, *Science 294*, 369−74.
23. Sawano, A., and Miyawaki, A. (2000) Directed evolution of green fluorescent protein by a new versatile PCR strategy for site-directed and semi-random mutagenesis, *Nucleic Acids Res. 28*, E78.
24. Bradford, M. M. (1976) A rapid and sensitive method for the quantitation of microgram quantities of protein utilizing the principle of protein-dye binding, *Anal. Biochem. 72*, 248−54.
25. Teng, T.-Y. (1990) Mounting of crystals for macromolecular crystallography in a free-standing thin film, *J. Appl. Crystallogr. 23*, 387−391.
26. Pohl, E., Ristau, U., Gehrmann, T., Jahn, D., Robrahn, B., Malthan, D., Dobler, H., and Hermes, C. (2004) Automation of the EMBL Hamburg protein crystallography beamline BW7B, *J. Synchrotron Radiat. 11*, 372−377.
27. Hermes, C., Gehrmann, T., Jahn, D., Ristau, U., Robrahn, B., and Siambanis, T. (2004) in *Synchrotron Radiation Instrumentation: Eight International Conference* (Warwick, T., Arthur, J., Padmore, H. A., and Stoehr, J., Eds.) pp 384−388, American Institute of Physics, Woodbury, NY.
28. Otwinowski, Z., and Minor, W. (1997) Processing of X-ray diffraction data collected in oscillation mode, *Methods Enzymol. 276*, 307−326.
29. Read, R. J. (1986) Improved Fourier coefficients for maps using phases from partial structures with errors, *Acta Crystallogr., Sect. A 42*, 140−149.
30. McRee, D. E. (1999) XtalView/Xfit--A versatile program for manipulating atomic coordinates and electron density, *J. Struct. Biol. 125*, 156−65.
31. Perrakis, A., Morris, R., and Lamzin, V. S. (1999) Automated protein model building combined with iterative structure refinement, *Nat. Struct. Biol. 6*, 458−63.
32. Jones, T. A., Zou, J. Y., Cowan, S. W., and Kjeldgaard, M. (1991) Improved methods for building protein models in electron density maps and the location of errors in these models, *Acta Crystallogr., Sect. A 47*, 110−119.
33. Kraulis, P. (1991) MOLSCRIPT: a program to produce both detailed and schematic plots of protein structures, *J. Appl. Crystallogr. 24*, 946−950.
34. Esnouf, R. M. (1997) An extensively modified version of MolScript that includes greatly enhanced coloring capabilities, *J. Mol. Graphics 15*, 132−134.
35. Brunger, A. T. (1992) Free R value: a novel statistical quantity for assessing the accuracy of crystal structures, *Nature 355*, 472−475.
36. Ramachandran, G. N., and Sasisekharan, V. (1968) Conformation of polypeptides and proteins, *Adv. Protein Chem. 23*, 283−438.
37. Wilmanns, M., Hyde, C. C., Davies, D. R., Kirschner, K., and Jansonius, J. N. (1991) Structural conservation in parallel beta/alpha-barrel enzymes that catalyze three sequential reactions in the pathway of tryptophan biosynthesis, *Biochemistry 30*, 9161−9.
38. Morris, A. J., and Tolan, D. R. (1994) Lysine-146 of rabbit muscle aldolase is essential for cleavage and condensation of the C3−C4 bond of fructose 1,6-bis(phosphate), *Biochemistry 33*, 12291−7.
39. Midelfort, C. F., Gupta, R. K., and Rose, I. A. (1976) Fructose 1,6-bisphosphate: isomeric composition, kinetics, and substrate specificity for the aldolases, *Biochemistry 15*, 2178−85.
40. Rose, I. A., and O'Connell, E. L. (1977) Specificity of fructose-1, 6-P2 aldolase (muscle) and partition of the enzyme among catalytic intermediates in the steady state, *J. Biol. Chem. 252*, 479−82.
41. Swenson, C. A., and Barker, R. (1971) Proportion of keto and aldehydo forms in solutions of sugars and sugar phosphates, *Biochemistry 10*, 3151−4.
42. Gray, G. R., and Barker, R. (1970) Studies on the substrates of D-fructose 1,6-diphosphate aldolase in solution, *Biochemistry 9*, 2454−62.
43. Winn, M. D., Isupov, M. N., and Murshudov, G. N. (2001) Use of TLS parameters to model anisotropic displacements in macromolecular refinement, *Acta Crystallogr.*, Sect. D 57, 122−133.

BI048192O